

Recent progress of magnetic reconnection research in the MAST spherical tokamak

H. Tanabe, T. Yamada, T. Watanabe, K. Gi, M. Inomoto, R. Imazawa, M. Gryaznevich, C. Michael, B. Crowley, N. J. Conway, R. Scannell, J. Harrison, I. Fitzgerald, A. Meakins, N. Hawkes, K. G. McClements, T. O'Gorman, C. Z. Cheng, Y. Ono, and

Citation: [Physics of Plasmas](#) **24**, 056108 (2017);

View online: <https://doi.org/10.1063/1.4977922>

View Table of Contents: <http://aip.scitation.org/toc/php/24/5>

Published by the [American Institute of Physics](#)

Articles you may be interested in

[Extended MHD modeling of tearing-driven magnetic relaxation](#)

[Physics of Plasmas](#) **24**, 056107 (2017); 10.1063/1.4977540

[Electron holes in phase space: What they are and why they matter](#)

[Physics of Plasmas](#) **24**, 055601 (2017); 10.1063/1.4976854

[A methodology for the rigorous verification of Particle-in-Cell simulations](#)

[Physics of Plasmas](#) **24**, 055703 (2017); 10.1063/1.4977917

[MHD modeling of a DIII-D low-torque QH-mode discharge and comparison to observations](#)

[Physics of Plasmas](#) **24**, 055902 (2017); 10.1063/1.4977467

[Analysis of self-consistent nonlinear wave-particle interactions of whistler waves in laboratory and space plasmas](#)

[Physics of Plasmas](#) **24**, 056501 (2017); 10.1063/1.4977539

[Energy conversion mechanism for electron perpendicular energy in high guide-field reconnection](#)

[Physics of Plasmas](#) **24**, 032901 (2017); 10.1063/1.4977908

**PHYSICS
TODAY**

**COMPLETELY
REDESIGNED!**

Physics Today Buyer's Guide
Search with a purpose.

Recent progress of magnetic reconnection research in the MAST spherical tokamak

H. Tanabe,^{1,a),b)} T. Yamada,² T. Watanabe,¹ K. Gi,¹ M. Inomoto,¹ R. Imazawa,³ M. Gryaznevich,^{4,c)} C. Michael,^{4,d)} B. Crowley,^{4,e)} N. J. Conway,⁴ R. Scannell,⁴ J. Harrison,⁴ I. Fitzgerald,⁴ A. Meakins,⁴ N. Hawkes,⁴ K. G. McClements,⁴ T. O'Gorman,⁴ C. Z. Cheng,⁵ Y. Ono,¹ and MAST Team⁴

¹Graduate School of Frontier Sciences, University of Tokyo, Tokyo 113-0032, Japan

²Faculty of Arts and Science, Kyushu University, Fukuoka 819-0395, Japan

³National Institutes for Quantum and Radiological Science and Technology, Ibaraki 311-0193, Japan

⁴CCFE, Culham Science Centre, Abingdon, Oxfordshire OX14 3DB, United Kingdom

⁵Institute of Space and Plasma Sciences, National Cheng Kung University, Tainan 70101, Taiwan

(Received 18 November 2016; accepted 16 February 2017; published online 6 March 2017)

In the last three years, magnetic reconnection research in the MAST spherical tokamak achieved major progress by the use of new 32 chord ion Doppler tomography and 130 channel YAG and 300 channel Ruby Thomson scattering diagnostics. In addition to the previously achieved high power plasma heating during merging, detailed full temperature profile measurements including the diffusion region have been achieved for the first time. 2D imaging measurements of ion and electron temperature profiles have revealed that magnetic reconnection mostly heats ions globally in the downstream region of outflow jet and electrons locally around the X -point. The toroidal field in MAST “over 0.3T” strongly inhibits cross-field thermal transport, and the characteristic peaked electron temperature profile around the X -point is sustained on a millisecond time scale. In contrast, ions are mostly heated in the downstream region of outflow acceleration and around the stagnation point formed by reconnected flux mostly by viscosity dissipation and shock-like compressional damping of the outflow jet. Toroidal confinement also contributes to the characteristic ion temperature profile, forming a ring structure aligned with the closed flux surface. There is an effective confinement of the downstream thermal energy due to a thick layer of reconnected flux. The characteristic structure is sustained for longer than an ion-electron energy relaxation time (~ 4 ms), and the energy exchange between ions and electrons contributes to the bulk electron heating in the downstream region. The toroidal guide field mostly contributes to the formation of a localized electron heating structure around the X -point but not to bulk ion heating downstream. © 2017 Author(s). All article content, except where otherwise noted, is licensed under a Creative Commons Attribution (CC BY) license (<http://creativecommons.org/licenses/by/4.0/>). [<http://dx.doi.org/10.1063/1.4977922>]

I. INTRODUCTION

Magnetic reconnection is a fundamental process, which converts the magnetic energy of anti-parallel reconnecting fields to kinetic and thermal energies of plasmas through the breaking and topological rearrangement of magnetic field lines.^{1,2} This process is known as an effective way of converting magnetic energy into plasma energy in proportion to the square of the reconnecting field $\propto B_{rec}^2$.³ Recent satellite observations of solar flares also revealed several important signatures of reconnection heating. In the solar flares, hard X-ray spots appear at loop-tops of coronas together with another two foot-point spots on the photosphere. The loop-top hot spots are considered to be caused by fast shocks

formed in the down-stream of reconnection outflow.⁴ The 2D imaging measurements of the Hinode spectrometer documented a significant broadening of the Ca line downstream of reconnection.⁵ These phenomena suggest direct ion heating by reconnection outflow. On the other hand, the V-shaped high electron temperature region was found around the X -line of reconnection as possible evidence of the slow shock structure.⁶

However, those heating characteristics of reconnection are still under serious discussion because of the absence of (or limited) *in-situ* diagnostics for astrophysical reconnection events. Since 1986, the merging of two toroidal plasmas (flux tubes) has been studied in a number of experiments: TS-3,^{7,8} START,⁹ MRX,¹⁰ SSX,¹¹ VTF,¹² TS-4,¹³ UTST,^{14,15} and MAST.¹⁶ For those laboratory experiments, evidence of plasma acceleration toward the outflow direction was observed as a split line-integrated distribution function in 0D,¹⁷ 1D, and 2D bidirectional toroidal acceleration during counter helicity spheromak merging^{18,19} and in-plane Mach probe measurement around the X -point with and without the guide field.^{20–22} In the recent TS-3 experiment, 2D ion and electron heating characteristics were revealed^{23,24} as bulk

Note: Paper DI2 2, Bull. Am. Phys. Soc. **61**, 116 (2016).

^{a)}Invited speaker.

^{b)}Electronic mail: tanabe@k.u-tokyo.ac.jp

^{c)}Present address: Tokamak Energy, Culham Innovation Centre, Abingdon, Oxfordshire OX14 3DB, United Kingdom.

^{d)}Present address: Research School of Physical Sciences and Engineering, Australian National University, Canberra 0200, Australia.

^{e)}Present address: DIII-D National Fusion Facility, General Atomics Court, California 92186-5608, USA.

heating of ions downstream and localized electron heating around the X -point. The energy inventory has been investigated in both push merging^{3,25} and pull reconnection.^{26,27} However, the electron temperature tends to be as low as 15 eV for most of the laboratory experiments due to a radiation barrier by low- Z impurities, the presence of invasive probe diagnostics inside the vessel, and convective loss under low guide field conditions.²⁸

The world's largest merging device MAST²⁹ (Mega Ampere Spherical Tokamak) achieved remarkable success in those issues. Reconnection heating exceeds ~ 1 keV at maximum both for ions²⁰ and electrons,³⁰ with individual ion energies ranging up to several tens of keV,³¹ pulse duration time exceeds 100 ms without solenoid,³² and the merging startup plasma is successfully connected to the quasi-steady and H-mode regime.³³ In addition, the spatial resolution of Ruby and YAG Thomson scattering (TS) systems has a significant advantage with 300 and 130 channels, respectively.^{34–36} In the last decade, the viewing range of ion temperature profile measurement was normally limited to $r > 0.8$ m due to the innermost impact radius of the neutral beam;^{37,38} however, from 2013 (M9 campaign), MAST-univ. Tokyo collaboration addressed this issue by the temporary repurposing of an existing collecting lens to provide a 32 chord tomographic ion Doppler spectroscopy capability on the midplane with a radial range spanning the diffusion region.^{3,23,39} Here, this paper addresses the recent major progress of detailed profile measurement of both electron and heating using those fine diagnostics during a high field reconnection experiment in MAST.

II. EXPERIMENTAL SETUP

Figure 1 illustrates the geometric setting of the merging/reconnection experiment in the MAST spherical tokamak (ST). As visualized in the fast camera images, P3 coils generate initial two toroidal plasma rings at the top and bottom of the vacuum vessel ($R_{\text{wall}} = 2.0$ m) and contribute to drive magnetic reconnection in MAST.^{33,41–44} The reconnected field forms a thick layer of the closed flux surface downstream, and the field line topology of two plasma rings is changed to a single spherical tokamak configuration after merging.^{3,20,24} The toroidal field is ~ 0.3 – 0.8 T the around diffusion region, and the reconnecting field is roughly $B_{\text{rec}} \sim 0.07$ – 0.15 T ($B_{\text{rec}} \sim B_p \propto I_p \propto I_{P3}$ ⁴⁵ based on equilibrium fitting/reconstruction (EFIT)⁴⁶ of the radial component of poloidal B_r field after magnetic reconnection at $t = 30$ ms), ion skin depth $c/\omega_{pi} \sim 0.1$ m, ion Larmor radius $\rho_i < 0.01$ m, and ion cyclotron frequency $\omega_{ci} > 10$ Mrad/s. P1 is center solenoid,⁴⁷ P2 generates double null divertor configuration after merging,⁴⁸ P4 and P5 control radial equilibrium,^{32,49} and P6 coils control the vertical position.⁵⁰

Two types of high resolution Thomson scattering (TS) systems, Nd:YAG (filter type) and Ruby (TV Thomson) were used to measure the electron temperature and density profiles at $z = -0.015$ m and $z = 0.015$ m with spatial resolutions of ~ 10 mm and ~ 15 mm, respectively, including optical blurring. The YAG-TS system uses 8 lasers for time resolved measurement for 8 time frames (usually 8×30 Hz operation) and has

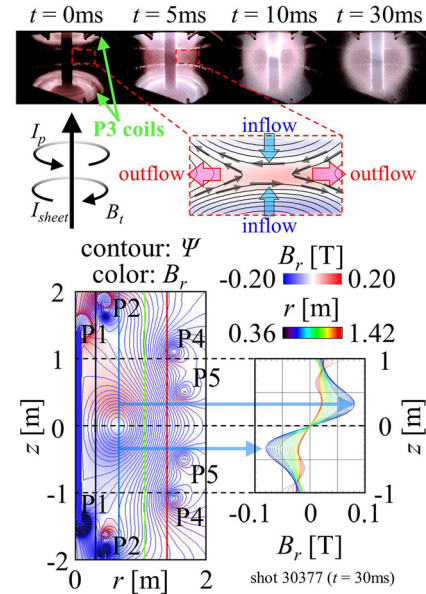


FIG. 1. Geometric setting of merging/reconnection in the MAST spherical tokamak. Two plasma rings generated around P3 coils are merged at the midplane ($z = 0$ m). The reference amplitude of the reconnecting magnetic field is estimated from EFIT reconstruction of the radial component of poloidal magnetic field B_r after merging.

5 spectral channels (central wavelength [nm]/bandwidth [nm]: 755/170, 917/155, 1017.5/45, 1047.5/15, and 1057.7/5.5). 36 spatial points were measured before the shot number of 22961, and the number was increased to 130 channels in 2009.³⁶ Ruby-TS (TV Thomson) measures a single time frame in a MAST pulse but has advantages of 300 spatial channels and 302 pixels for wavelength ranging $585.10 < \lambda < 901.15$ nm with an instrumental function of ~ 10 nm (FWHM) and is used for the confirmation of thermalized electron distribution.^{34,35}

In 2013, a new dedicated ion temperature measurement was installed on the midplane ($z = 0$ mm) with the viewing range of $0.25 \text{ m} < r < 1.1$ m to cover the full reconnection region.³⁹ As shown in Fig. 2, the diagnostic system is composed of a collecting lens ($f = 200$ mm) and optical fibers (400 μm core (silica); NA = 0.22 and 40 m long: the existing equipment^{37,51,52} was temporarily moved from the sector 7 to the sector 9 midplane viewing port), 32 channel new patch fibers (400 μm core (silica); NA = 0.22 and 5 m long) to transfer the collected spectra to a Czerny-Turner grating spectrometer (focal length $f = 1.0$ m, grating frequency $g = 1800$ L/mm, slit width 200 μm), input optics ($f = 75$ mm and 100 mm), magnifying optics ($f_1 = 75$ mm and 75 mm; $f_{\text{space}} = 75$ mm and 30 mm) for the correction of astigmatism, and an EMCCD (electron multiplying CCD: Princeton Instruments: 512×512 pixels, 16 $\mu\text{m}/\text{pixel}$, 2.65 ms/frame for binned 32 spectra and 230.4 μs for the image shift time). For the fast frame rate operation, a ferroelectric liquid crystal FLC shutter was used to reduce the smearing effect, which causes cross-talk for neighboring spectra in the CCD image. In the experiment, the CVI line ($\text{C}^{5+}; \lambda = 529.05$ nm) is mainly used, and the time evolution of 32 channel spectra is recorded by 512 pixel wavelength channels typically with 0.0078 nm/pixel.³⁹

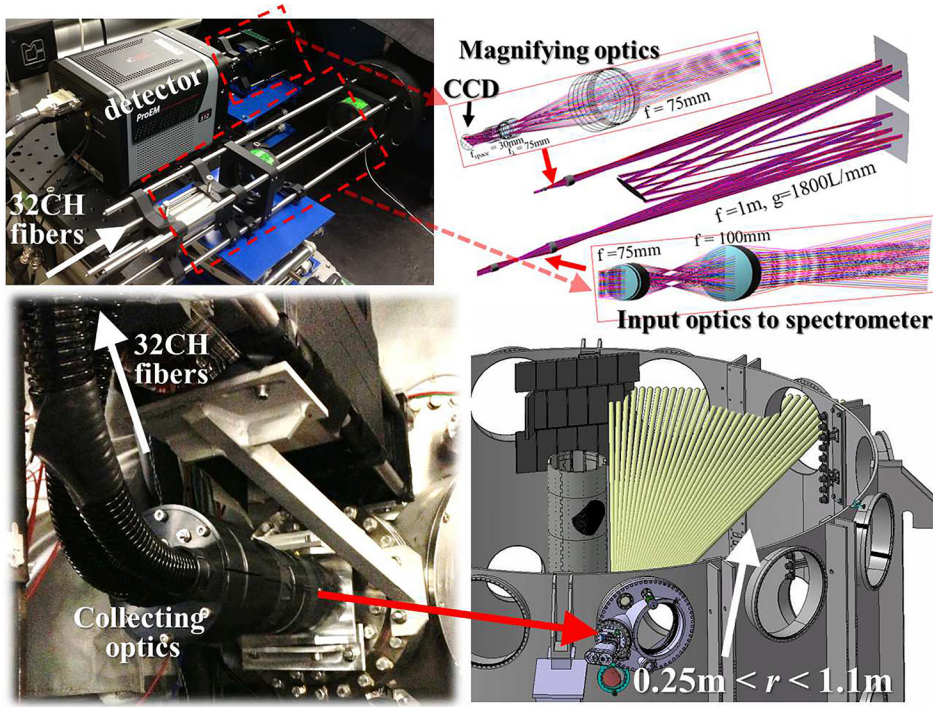


FIG. 2. 32CH ion Doppler tomography diagnostics system composed of collecting optics (viewing range in $0.25\text{ m} < r < 1.1\text{ m}$), optical fibers, Czerny-Turner spectrometer ($f=1.0\text{ m}$) with optimized imaging optics, and a CCD detector.

III. RECONNECTION HEATING DURING THE MERGING PLASMA STARTUP EXPERIMENT

Figure 3 shows the time evolution of the typical discharge waveform of plasma current I_p and reconnection driving coil current I_{P3} , a magnetic diagnostics signal dB_z/dt ($r \sim 0.2\text{ m}$, $z \sim 0\text{ m}$ (Ref. 53)), plasma outer midplane separatrix radius r_{sep} that is monitored by a 2048 pixel linear D_α camera ranging $r < 1.8\text{ m}$ (Ref. 54), and Thomson scattering measurement of electron temperature and density profiles in the shot 25740 ($r_{\text{sep}} \sim 1.0\text{ m}$, $B_{\text{rec}} \sim 0.11\text{ T}$, and $B_t \sim 0.6\text{ T}$:

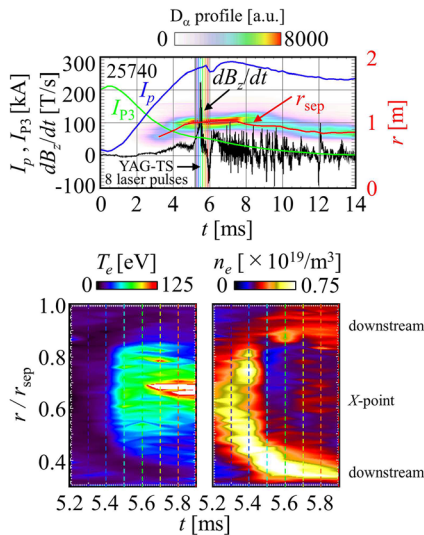


FIG. 3. Typical waveform of I_{P3} , I_p , r_{sep} , and dB_z/dt during merging plasma startup and Thomson scattering measurement of T_e and n_e profiles. During magnetic reconnection, a large dB_z/dt signal was observed by boundary Mirnov coil measurement around $r \sim 0.2\text{ m}$, which indicates the change of the B_z component by reconnected flux. T_e forms a peaked structure during the oscillation, and n_e detects particle transport to the outflow direction from the X-point.

high guide field limit⁵⁵). The P3 ramp down current I_{P3} contributes to the formation of initial two plasma rings, and magnetic reconnection starts around 5 ms with a large spike of the dB_z/dt signal. For the merging/reconnection configuration, the B_r field corresponds to the reconnecting field and B_z is affected by the reconnected field, and then dB_z/dt detects downstream reconnected flux and has a large spike in microsecond time scale. During this event, 130 channel Thomson scattering measurement of n_e and T_e was performed at 8 time frames with the interval of 0.1 ms. Before merging ($t = 5.2, 5.3\text{ ms}$), electron temperature is as low as $\sim 10\text{ eV}$ and electron density has a peak around the X-point. After $t = 5.4\text{ ms}$, electron temperature rapidly increases at $t = 5.5\text{ ms}$ when the dB_z/dt signal reaches its maximum and then formed peaked distribution around the X-point where a higher parallel electric field should exist,^{56–58} while the built up electron density around the X-point is transported radially in the outflow region. For the closed flux type reconnection of spherical tokamak (ST) merging, outflow acceleration is damped at downstream and forms a double peak profile with shock-like steep density gradient.

Figure 4 shows 2D electron temperature and density profiles during discharges 21374–21380 (P6 coils are used to shift the vertical position of Thomson scattering measurement⁵⁰) after the fast reconnection event ($1.2\text{ m} < r_{\text{sep}} < 1.3\text{ m}$ for the vertical scan shots at $t = 8, 9, 10, 11, 12\text{ ms}$). The electron temperature profile forms a characteristic peaked structure around the X-point where localized electron acceleration and heating by the parallel electric field are reported in the high guide field laboratory merging (driven reconnection) experiment in UTST (University of Tokyo Spherical Tokamak),^{59–61} while the electron density increases downstream. In contrast to the no guide field experiment in MRX^{27,28} where electron energy gain is quickly transported downstream, the higher toroidal field in MAST strongly

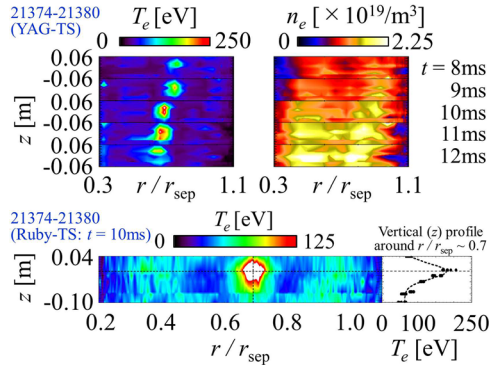


FIG. 4. 2D YAG Thomson scattering measurement of electron temperature and density profiles at $t = 8, 9, 10, 11, 12$ ms and Ruby Thomson scattering measurement at $t = 10$ ms. Magnetic reconnection heats electrons locally around the X-point ($r/r_{\text{sep}} \sim 0.7$) and also in the outflow region where the electron density increases.

inhibits the perpendicular heat conduction if, as expected, this scales as of $1/B_t^2$, and the established profile is sustained in millisecond time scale. At $t = 10$ ms, cross-validation with the 300 channel Ruby Thomson scattering measurement is also performed and successfully reproduces the highly localized hot spot around the X-point (peak width is roughly ~ 0.06 m $< c/\omega_{pi} \sim 0.1$ m) with Maxwellian velocity distribution. On the other hand, the electron temperature profile also forms characteristic high T_e area downstream. It is located around the high density region where reconnection outflow should dissipate by the effect of energy relaxation between electrons and ions to equilibrate both temperatures (for example, $\tau_{ei}^E \sim 4$ ms for $n_e \sim 1 \times 10^{19}/\text{m}^3$ and $T_e \sim 100$ eV).

Figure 5 shows the time evolution of the ion temperature profile. Magnetic reconnection increases ion temperature in the downstream region and more in the high field side. The ion temperature continues to increase downstream for several milliseconds because flow energy is being converted into thermal energy (energy equilibration time both between ion-ion and ion-impurity is shorter than 1 ms for $T_i \sim 200$ eV and $n_e \sim 1 \times 10^{19}/\text{m}^3$: isotropic rather than anisotropic heating^{62,63}). Figure 6 illustrates the 2D ion temperature profile in 30366–30368 and 30376–30377. Ion heating mainly occurs in the downstream region globally due to conversion of plasma outflow energy into thermal energy mostly by viscosity dissipation^{10,27} and shock-like compressional damping of outflow jet^{20,24} as in the two fluid simulation, which includes such fundamental collisional viscous dissipation.^{43,44} Smaller

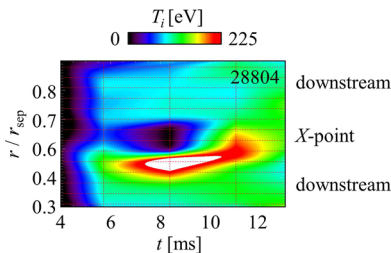


FIG. 5. Time evolution of the ion temperature profile. Magnetic reconnection heats ions in the downstream region and more in the high field side. Ion heating continues for several milliseconds during the conversion of flow energy into thermal energy.

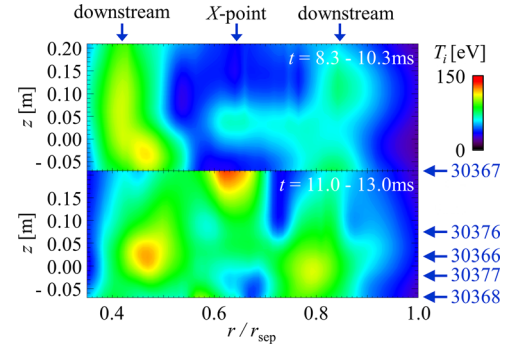


FIG. 6. 2D structure of ion temperature profiles at $t = 8.3\text{--}10.3$ ms and $11.0\text{--}13.0$ ms. Ion heating mainly occurs in the downstream region globally, while smaller ion heating also occurs around the X-point.

ion heating also occurs around the X-point by electron-ion energy equilibration. For the high guide field reconnection experiment in MAST, the ratio of collisional thermal diffusivities $\chi_{\parallel}^i/\chi_{\perp}^i \sim 2(\omega_{ci}\tau_{ii})^2 \gg 10$ is much higher than that of other laboratory experiments ($\chi_{\parallel}^i/\chi_{\perp}^i \sim 1$ for the no guide field experiment in MRX (magnetic reconnection experiment)⁶⁴). Thus, the better confinement also contributes to the characteristic temperature profile, and outflow heating downstream forms a ring structure of the closed flux surface,^{43,44} enhances the local energy relaxation between ions and electrons in the millisecond time scale of τ_{ei}^E , and finally contributes to the electron heating in the outflow region.

IV. COMPARISON OF ELECTRON AND ION HEATING

Figure 7 shows the time evolution of more detailed radial profiles of T_e , n_e , and T_i in the comparable time scale of electron-ion energy equilibration time ($\tau_{ei}^E \sim 4$ ms for $n_e \sim 1 \times 10^{19}/\text{m}^3$ and $T_e = 100$ eV). Before merging (black), both

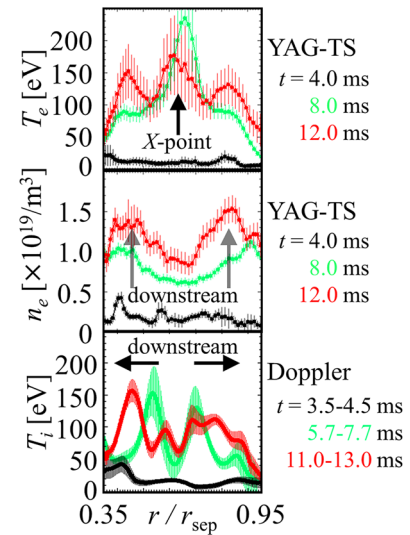


FIG. 7. Detailed 1D radial profile measurement of electron temperature, density, and ion temperature inside the diffusion region for three characteristic time frames (CIII line ($\text{C}^{2+}; \lambda = 464.7$ nm) is used at the time frame of $t = 3.5\text{--}4.5$ ms): (1) before merging (black), (2) just after the fast reconnection event (green), and (3) after electron-ion energy equilibration time (red). Magnetic reconnection heats electrons around the X-point and ions downstream. Both profiles finally form triple peaks through the energy transfer between ions and electrons with the delay of $\tau_{ei}^E \sim 4$ ms.

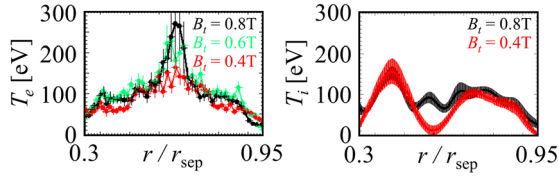


FIG. 8. Comparison of electron and ion temperature profiles with different toroidal guide field conditions. The structure of the peaked T_e profile becomes steeper with better confinement under high guide field conditions and also contributes to ion heating around the X-point by $T_i - T_e$ energy transfer, while the downstream ion temperature does not change.

temperatures are as low as ~ 10 eV. Just after reconnection (green), electrons are mainly heated around the X-point, while electron density and ion temperature profiles form double peaks in the outflow region. The characteristic different temperature distribution for both is relaxed to each other with millisecond time scale by the collisional coupling between ions and electrons; the electron temperature also increases downstream and ions around the X-point. Finally, both profiles form triple peaks around the X-point and downstream at $t \sim 12$ ms (red).

Figure 8 shows the effect of the guide field for electron and ion heating at the characteristic time frame of $t = 8$ ms for T_e and $t \sim 12$ ms for T_i , respectively. Both electron and ion temperatures around the X-point increase under higher guide field conditions probably because the higher toroidal field strongly inhibits cross-field thermal transport (scaling as $1/B_t^2$), so that the electrons remain in the region of a high toroidal electric field for longer. With the better confinement, such characteristic distribution also affects the ion temperature profile around the X-point. Because the perpendicular heat conduction of ions is expected to scale as $1/B_t^2$, ions also gain energy around the X-point under higher guide field conditions, finally forming a triple peak structure. On the other hand, downstream ion heating does not change as demonstrated in the push (driven) ST merging experiment with intermittent plasmoid ejection in TS-3^{3,65} and PIC (particle-in-cell) simulation with a driving electric field.^{56–58} For the operation range of ultra high guide field conditions $B_t > 0.3$ T and $B_t/B_{rec} > 3$ in MAST, outflow dissipation by viscosity damping is suppressed,^{66,67} however, the improved confinement by a higher guide field assists the confinement time of ions in a downstream local closed flux surface and finally damps outflow, and the dissipated flow energy heats ions downstream.

V. CONCLUSION

In the last three years, magnetic reconnection research in the MAST spherical tokamak achieved major progress through the use of new 32 chord ion Doppler tomography and 130 channel YAG and 300 channel Ruby Thomson scattering diagnostics. 2D detailed imaging measurement of both electron and ion temperature profiles around the diffusion region has been achieved for the first time. The new findings in the last three years are summarized as follows:

- High guide field reconnection heats electrons locally around the X-point.
- Ions are heated globally downstream through the dissipation of flow energy of outflow jet and formed ring structure around the closed flux surface downstream.

- Both T_e and T_i profiles form triple peaks in the thermal relaxation phase by electron-ion energy relaxation.
- Larger B_t produces higher T_e around the X-point but has a negligible effect on ion heating downstream by better toroidal confinement.

With the better confinement of reconnection heating under high guide field conditions ($B_t > 0.3$ T) and high temperature experimental conditions, which reduces the severe loss by collisional/radiation cooling, the results from MAST clearly revealed the characteristics of reconnection heating, namely, for electron heating as the highly localized peaked structure around the X-point. Ion heating also forms a clear structure of the confinement of outflow heating downstream for the toroidal merging configuration of magnetic reconnection. The fundamental energy equilibration process between ions and electrons after reconnection, which has not been clearly observed even after merging for short pulse laboratory experiments and astrophysical plasma, also affects both temperature profiles with comparable time scale to τ_{ei}^E , and both electron and ion temperature profiles form triple peak distribution. The toroidal guide field mainly contributes to the formation of the peaked electron temperature profile around the X-point and its contribution to the ion temperature profile while ion heating downstream does not change. Although the absence of direct magnetic probe measurement for the hot plasma limits the detailed discussion of the formation mechanism of the characteristic heating profile, it should be noted that the ultra-fine non-invasive optical diagnostics in MAST successfully reveal the existence of a highly peaked electron temperature profile around the X-point without breaking the structure whose scale is comparable to typical invasive probe diagnostics. In addition, the achieved bulk (downstream) electron temperature became comparable order to ion temperature after the delay of τ_{ei}^E and succeeded in pioneering the application of reconnection heating for CS-less startup of spherical tokamak even in the ultrahigh guide field regime ($B_t > 0.3$ T), which is preferable for better confinement in practical operation.

ACKNOWLEDGMENTS

This work was supported by Grant-in-Aid for Scientific Research 22246119, 22656208, 25820434, 15H05750, and 15K20921, JSPS Core-to-Core program 22001, JSPS institutional Program for Young Researcher Overseas Visits, and NIFS Collaboration Research Programs (NIFS11KNWS001, NIFS11KLEH024 and NIFS11KUTR060). This work was also partly funded by the RCUK Energy Programme under Grant No. EP/I501045 and the European Communities. The views and opinions expressed herein do not necessarily reflect those of the European Commission. We acknowledge Adam Stanier and Alan Sykes for useful discussion and Samuli Saarelma, Ian Chapman, and Brian Lloyd for managing the campaign shots for the reconnection studies.

¹M. Yamada, R. Kulsrud, and H. Ji, *Rev. Mod. Phys.* **82**, 603 (2010).

²E. G. Zweibel and M. Yamada, "Magnetic reconnection in astrophysical and laboratory plasmas," *Annu. Rev. Astron. Astrophys.* **47**, 291 (2009).

- ³Y. Ono, H. Tanabe, T. Yamada, K. Gi, T. Watanabe, T. Ii, M. Gryaznevich, R. Scannell, N. Conway, B. Crowley, and C. Michael, *Phys. Plasmas* **22**, 055708 (2015).
- ⁴S. Masuda, T. Kosugi, H. Hara, S. Tsuneta, and Y. Ogawara, *Nature* **371**, 495 (1994).
- ⁵H. Hara, T. Watanabe, L. K. Harra, J. L. Culhane, and P. R. Young, *Astrophys. J.* **741**, 107 (2011).
- ⁶T. Shimizu, S. Tsuneta, L. W. Acton, J. R. Lemen, Y. Ogawara, and Y. Uchida, *Astrophys. J.* **422**, 906 (1994).
- ⁷Y. Ono, A. Yumoto, and M. Katsurai, in *Proceedings of the 1986 IEEE International Conference on Plasma Science, Saskatoon, Canada, 1986* (IEEE, New York, 1986), p. 77.
- ⁸Y. Ono, A. Morita, M. Katsurai, and M. Yamada, *Phys. Fluids B* **5**, 3691 (1993).
- ⁹M. Gryaznevich, R. Akers, P. G. Carolan, N. J. Conway, D. Gates, A. R. Field, T. C. Hender, I. Jenkins, R. Martin, M. P. S. Nightingale, C. Ribeiro, D. C. Robinson, A. Sykes, M. Tourmianski, M. Valovic, and M. J. Walsh, *Phys. Rev. Lett.* **80**, 3972 (1998).
- ¹⁰M. Yamada, H. Ji, S. Hsu, T. Carter, R. Kulsrud, N. Bretz, F. Jobs, Y. Ono, and F. Perkins, *Phys. Plasmas* **4**, 1936 (1997).
- ¹¹M. R. Brown, *Phys. Plasmas* **6**, 1717 (1999).
- ¹²J. Egedal, A. Fasoli, M. Porkolab, and D. Tarkowski, *Rev. Sci. Instrum.* **71**, 3351 (2000).
- ¹³Y. Ono, T. Kimura, E. Kawamori, Y. Murata, S. Miyazaki, Y. Ueda, M. Inomoto, A. L. Balandin, and M. Katsurai, *Nucl. Fusion* **43**, 789 (2003).
- ¹⁴T. Yamada, R. Imazawa, S. Kamio, R. Hihara, K. Abe, M. Sakumura, Q. Cao, T. Oosako, H. Kobayashi, T. Wakatsuki, B. An, Y. Nagashima, H. Sakakita, H. Koguchi, S. Kiyama, Y. Hirano, M. Inomoto, A. Ejiri, Y. Takase, and Y. Ono, *Plasma Fusion Res.* **5**, S2100 (2010).
- ¹⁵M. Inomoto, T. G. Watanabe, K. Gi, K. Yamasaki, S. Kamio, R. Imazawa, T. Yamada, X. Guo, T. Ushiki, H. Ishikawa, H. Nakamata, N. Kawakami, T. Sugawara, K. Matsuyama, K. Noma, A. Kuwahata, and H. Tanabe, *Nucl. Fusion* **55**, 033013 (2015).
- ¹⁶M. Gryaznevich, R. J. Akers, G. F. Counsell, G. Cunningham, A. Dnestrovskij, A. R. Field, T. C. Hender, A. Kirk, B. Lloyd, H. Meyer, A. W. Morris, A. Sykes, A. Tabasso, M. Valovic, G. M. Voss, H. R. Wilson, and MAST and NBI Teams, *Phys. Plasmas* **10**, 1803 (2003).
- ¹⁷T. Gray, V. S. Lukin, M. R. Brown, and C. D. Cothran, *Phys. Plasmas* **17**, 102106 (2010).
- ¹⁸Y. Ono, M. Yamada, T. Akao, T. Tajima, and R. Matsumoto, *Phys. Rev. Lett.* **76**, 3328 (1996).
- ¹⁹H. Tanabe, H. Oka, M. Annoura, A. Kuwahata, K. Kadowaki, Y. Kaminou, S. You, A. Balandin, M. Inomoto, and Y. Ono, *Plasma Fusion Res.* **8**, 2405088 (2013).
- ²⁰Y. Ono, H. Tanabe, T. Yamada, M. Inomoto, T. Ii, S. Inoue, K. Gi, T. Watanabe, M. Gryaznevich, R. Scannell, C. Michael, and C. Z. Cheng, *Plasma Phys. Controlled Fusion* **54**, 124039 (2012).
- ²¹J. Yoo, M. Yamada, H. Ji, J. Jara-Almonte, C. E. Myers, and L. J. Chen, *Phys. Rev. Lett.* **113**, 095002 (2014).
- ²²J. Yoo, M. Yamada, H. Ji, and C. E. Myers, *Phys. Rev. Lett.* **110**, 215007 (2013).
- ²³H. Tanabe, A. Kuwahata, H. Oka, M. Annoura, H. Koike, K. Nishida, S. You, Y. Narushima, A. Balandin, M. Inomoto, and Y. Ono, *Nucl. Fusion* **53**, 093027 (2013).
- ²⁴Y. Ono, H. Tanabe, Y. Hayashi, T. Ii, Y. Narushima, T. Yamada, M. Inomoto, and C. Z. Cheng, *Phys. Rev. Lett.* **107**, 185001 (2011).
- ²⁵Y. Ono, M. Inomoto, T. Okazaki, and Y. Ueda, *Phys. Plasmas* **4**, 1953 (1997).
- ²⁶S. C. Hsu, G. Fiksel, T. A. Carter, H. Ji, R. M. Kulsrud, and M. Yamada, *Phys. Rev. Lett.* **84**, 3859 (2000).
- ²⁷M. Yamada, J. Yoo, J. Jara-Almonte, H. Ji, R. M. Kulsrud, and C. E. Myers, *Nat. Commun.* **5**, 4774 (2014).
- ²⁸J. Yoo, M. Yamada, H. Ji, J. Jara-Almonte, and C. E. Meyers, *Phys. Plasmas* **21**, 055706 (2014).
- ²⁹B. Lloyd, R. J. Akers, F. Alladio, S. Allan, L. C. Appel, M. Barnes, N. C. Barratt, N. Ben Ayed, B. N. Breizman, M. Cecconello *et al.*, *Nucl. Fusion* **51**, 094013 (2011).
- ³⁰T. Yamada, H. Tanabe, T. G. Watanabe, Y. Hayashi, R. Imazawa, M. Inomoto, Y. Ono, M. Gryaznevich, R. Scannell, C. Michael, and MAST Team, *Nucl. Fusion* **56**, 106019 (2016).
- ³¹K. G. McClements and M. R. Turnyanskiy, *Plasma Phys. Controlled Fusion* **59**, 014012 (2017).
- ³²M. Gryaznevich, *IEEE Trans. Fund. Mater.* **125**, 881 (2005).
- ³³A. Sykes, R. J. Akers, L. C. Appel, E. R. Arends, P. G. Carolan, N. J. Conway, G. F. Counsell, G. Cunningham, A. Dnestrovskij, and Yu. N. Dnestrovskij, *Nucl. Fusion* **41**, 1423 (2001).
- ³⁴M. J. Walsh, E. R. Arends, P. G. Carolan, M. R. Dunstan, M. J. Forrest, S. K. Nielsen, and R. O'Gorman, *Rev. Sci. Instrum.* **74**, 1663 (2003).
- ³⁵E. R. Arends, see <https://www.differ.nl/node/1512> for Ph.D. thesis, Eindhoven University of Technology, 2003.
- ³⁶R. Scannell, M. J. Walsh, M. R. Dunstan, J. Figueiredo, G. Naylor, T. O'Gorman, S. Shibaev, K. J. Gibson, and H. Wilson, *Rev. Sci. Instrum.* **81**, 10D520 (2010).
- ³⁷N. J. Conway, P. G. Carolan, J. McCone, M. J. Walsh, and M. Wisse, *Rev. Sci. Instrum.* **77**, 10F131 (2006).
- ³⁸A. Sykes, F. Alladio, P. Costa, N. Conway, G. Cunningham, A. Dnestrovskij, M. Gryaznevich, J. Hicks, M. Hood, A. Mancuso, G. McArdle, P. Micozzi, M. Price, F. Volpe, M. J. Walsh, and M. Wisse, in *Proceedings of the 32nd EPS Conference on Plasma Physics, Tarragona, 2005* (EPS, Tarragona, 2005), P-4.112.
- ³⁹H. Tanabe, T. Yamada, T. Watanabe, K. Gi, K. Kadowaki, M. Inomoto, R. Imazawa, M. Gryaznevich, R. Scannell, N. Conway, B. Crowley, K. G. McClements, I. Fitzgerald, C. Michael, J. Harrison, A. Meakins, N. Hawkes, T. O'Gorman, C. Z. Cheng, and Y. Ono, *Plasma Fusion Res.* **11**, 1302093 (2016).
- ⁴⁰A. Kirk, N. Ben Ayed, G. Counsell, B. Dudson, T. Eich, A. Herrmann, B. Koch, R. Martin, A. Meakins, S. Saarelma, R. Scannell, S. Tallents, M. Walsh, H. R. Wilson, and MAST Team, *Plasma Phys. Controlled Fusion* **48**, B433 (2006).
- ⁴¹A. Stanier, P. Browning, M. Gordovskyy, K. G. McClements, M. P. Gryaznevich, and V. S. Lukin, *Phys. Plasmas* **20**, 122302 (2013).
- ⁴²P. K. Browning, A. Stanier, G. Ashworth, K. G. McClements, and V. S. Lukin, *Plasma Phys. Controlled Fusion* **56**, 064009 (2014).
- ⁴³A. Stanier, see <https://www.escholar.manchester.ac.uk/jrnl/item/?pid=uk-ac-man-scw:211308> for Ph.D. thesis, The University of Manchester, 2013, p. 203.
- ⁴⁴P. K. Browning, S. Cardnell, M. Evans, F. Arese Lucini, V. S. Lukin, K. G. McClements, and A. Stanier, *Plasma Phys. Controlled Fusion* **58**, 014041 (2016).
- ⁴⁵H. Tanabe, T. Yamada, T. Watanabe, K. Gi, K. Kadowaki, M. Inomoto, R. Imazawa, M. Gryaznevich, C. Michael, B. Crowley, N. J. Conway, R. Scannell, J. Harrison, I. Fitzgerald, A. Meakins, N. Hawkes, K. G. McClements, T. O'Gorman, C. Z. Cheng, Y. Ono, and MAST Team, *Phys. Rev. Lett.* **115**, 215004 (2015).
- ⁴⁶L. L. Lao, H. St. John, R. D. Stambaugh, A. G. Kellman, and W. W. Pfeiffer, *Nucl. Fusion* **25**, 1611 (1985).
- ⁴⁷M. Cox and MAST Team, *Fusion Eng. Des.* **46**, 397 (1999).
- ⁴⁸B. Lloyd, J. W. Ahn, R. J. Akers, L. C. Appel, E. R. Arends, K. B. Axon, R. J. Buttery, C. Byrom, P. G. Carolan, and C. Challis, *Nucl. Fusion* **43**, 1665 (2003).
- ⁴⁹I. T. Chapman, J. Adamek, R. J. Akers, S. Allan, L. Appel, O. Asunta, M. Barnes, N. Ben Ayed, T. Bigelow, W. Boeglin *et al.*, *Nucl. Fusion* **55**, 104008 (2015).
- ⁵⁰G. Cunningham, *Fusion Eng. Des.* **88**, 3238 (2013).
- ⁵¹C. Michael, N. Conway, B. Crowley, O. Jones, W. W. Heidbrink, S. Pinches, E. Braeken, R. Akers, C. Challis, M. Turnyanskiy, A. Patel, D. Muir, R. Gaffka, and S. Bailey, *Plasma Phys. Controlled Fusion* **55**, 095007 (2013).
- ⁵²S. Henderson, L. Garzotti, F. J. Casson, D. Dickinson, M. O'Mullane, A. Patel, C. M. Roach, H. P. Summers, H. Tanabe, M. Valovič, and MAST Team, *Plasma Phys. Controlled Fusion* **57**, 095001 (2015).
- ⁵³T. Edlington, R. Martin, and T. Pinfold, *Rev. Sci. Instrum.* **72**, 421 (2001).
- ⁵⁴J. Storrs, J. Dowling, G. Counsell, and G. McArdle, *Fusion Eng. Des.* **81**, 1841 (2006).
- ⁵⁵J. T. Dahlin, J. F. Drake, and M. Swisdak, *Phys. Plasmas* **23**, 120704 (2016).
- ⁵⁶S. Inoue, Y. Ono, H. Tanabe, R. Horiuchi, and C. Z. Cheng, *Nucl. Fusion* **55**, 083014 (2015).
- ⁵⁷C. Z. Cheng, S. Inoue, Y. Ono, and R. Horiuchi, *Phys. Plasmas* **22**, 101205 (2015).
- ⁵⁸C. Z. Cheng, S. Inoue, Y. Ono, and R. Horiuchi, *Plasma Fusion Res.* **11**, 1401081 (2016).
- ⁵⁹X. Guo, M. Inomoto, T. Sugawara, K. Yamasaki, T. Ushiki, Y. Ono, and TS Group, *Phys. Plasmas* **22**, 101201 (2015).
- ⁶⁰K. Yamasaki, S. Inoue, S. Kamio, T. G. Watanabe, T. Ushiki, X. Guo, T. Sugawara, K. Matsuyama, N. Kawakami, T. Yamada, M. Inomoto, and Y. Ono, *Phys. Plasmas* **22**, 101202 (2015).

- ⁶¹T. Ushiki, M. Inomoto, K. Yamasaki, X. Guo, T. Sugawara, K. Matsuyama, H. Koguchi, and T. Yamada, [Plasma Fusion Res.](#) **11**, 2402100 (2016).
- ⁶²T. D. Phan, J. F. Drake, M. A. Shay, J. T. Gosling, G. Paschmann, J. P. Eastwood, M. Oieroset, M. Fujimoto, and V. Angelopoulos, [Geophys. Res. Lett.](#) **41**, 7002, doi:10.1002/2014GL061547 (2014).
- ⁶³J. F. Drake and M. Swisdak, [Phys. Plasmas](#) **21**, 072903 (2014).
- ⁶⁴A. Kuritsyn, Ph.D. thesis, Princeton University, 2005, p. 125.
- ⁶⁵Y. Ono, Y. Hayashi, T. Ii, H. Tanabe, S. Ito, A. Kuwahata, T. Ito, Y. Kamino, T. Yamada, M. Inomoto, and TS-Group, [Phys. Plasmas](#) **18**, 111213 (2011).
- ⁶⁶S. I. Braginskii, in *Reviews of Plasma Physics*, edited by M. A. Leontovich (Consultants Bureau, New York, 1965), Vol. 1, p. 205.
- ⁶⁷Z. Yoshida, [Nucl. Fusion](#) **31**, 386 (1991).